Current Optics and Photonics
Vol. 1, No. 1, February 2017, pp. 65-72

ISSN: 2508-7266(Print) / ISSN: 2508-7274(Online)
DOI: https://doi.org/10.3807/COPP.2017.1.1.065

Low-loss Electrically Controllable Vertical Directional Couplers

Thang Q. Tran and Sangin Kim*

Department of Electrical and Computer Engineering, Ajou University, Suwon 16499 South Korea

(Received November 09, 2016 : revised December 21, 2016 : accepted December 21, 2016)

We propose a nearly lossless, compact, electrically modulated vertical directional coupler, which is based on the controllable evanescent coupling in a previously proposed graphene-assisted total internal reflection (GA-FTIR) scheme. In the proposed device, two single-mode waveguides are separate by graphene-SiO_2-graphene layers. By changing the chemical potential of the graphene layers with a gate voltage, the coupling strength between the waveguides, and hence the coupling length of the directional coupler, is controlled. Therefore, for a properly chosen, fixed device length, when an input wave is launched into one of the waveguides, the ratio of their output powers can be controlled electrically. The operation of the proposed device is analyzed, with the dispersion relations calculated using a model of a one-dimensional slab waveguide. The supermodes in the coupled waveguide are calculated using the finite-element method to estimate the coupling length, realistic devices are designed, and their performance was confirmed using the finite-difference time-domain method. The designed 3 μm by 1 μm device achieves an insertion loss of less than 0.11 dB, and a 24-dB extinction ratio between bar and cross states. The proposed low-loss device could enable integrated modulation of a strong optical signal, without thermal buildup.

Keywords : Directional coupler, Numerical modeling, Graphene
OCIS codes : (230.2090) Electro-optical devices; (230.3120) Integrated optics devices; (230.4110) Modulators; (230.4170) Multilayers

I. INTRODUCTION

Electrically controllable directional couplers find many applications, such as modulators, switches, and variable tappers. In particular, a fast and compact integrated electro-optical modulator is one of the key components of future optical computing [1]. Electrically controllable directional couplers can be realized using electro-optical materials, but the electro-optic coefficients of dielectric materials are typically quite small, so that a long device (several millimeters) is required.

Recently, the two-dimensional material graphene has drawn a lot of attention, because its electro-optical properties can be tuned drastically via gate voltage [2]. Therefore, many graphene-based electro-optical switching schemes have been proposed and investigated, theoretically [3, 4] and experimentally [5-7]. Their operating frequencies span from terahertz [4, 5] to the near-infrared optical-communication wavelength [3, 6, 7]. Most of them, however, rely on optical absorption to modulate incoming signals. While several such techniques have been realized experimentally [5-7], the thermal buildup resulting from such optical absorption could present a fundamental limit, preventing future very-large-scale integration of millions of such devices onto a single electro-optical integrated chip.

An interferometer-based optical switch could potentially operate without such optical loss [8-10]. However, such devices either are quite large [8, 9], due to the difficulty of modulating the refractive index of the guiding material, or are based on guided surface plasmon polaritons (SPPs) [10], introducing large propagation losses of their own, requiring additional plasmonic couplers and complicating integration with silicon photonics.

Recently, it has been numerically demonstrated that, by adding doped graphene layers to a frustrated total internal reflection (FTIR) structure, it is possible to directly control

*Corresponding author: sangin@ajou.ac.kr

Color versions of one or more of the figures in this paper are available online.

the evanescent coupling strength between the media by electrically controlling the epsilon of graphene in an epsilon-near-zero (ENZ) regime; this was dubbed a graphene-assisted (GA) FTIR structure [11]. It was shown that the optical behavior of the GA-FTIR structure could be tuned drastically, from close to optical insulation (zero coupling) at the ENZ frequency, to near-perfect tunneling (perfect coupling) at a frequency slightly below than the ENZ point [11]. (The ENZ frequency is defined as the frequency at which the magnitude of the complex permittivity of graphene becomes minimal, which varies as a function of the chemical potential of graphene, E_F [11].) Thus, if such a GA-FTIR configuration were applied to two coupled waveguides, it is expected that very different supermodes would form for the zero- and perfect-coupling regimes, enabling a very compact, electrically controllable directional coupler.

In this work, a compact electrically controllable vertical directional coupler based on the GA-FTIR configuration is numerically demonstrated. Since multilayered electrical integrated circuits [12-14] are the prevailing industrial technology, future intrachip optical interconnects should be adapted to the multilayered structure, and an optical inter-layer routing scheme will be needed. The proposed device, acting as a bidirectional switchable router between the layers of optical integrated circuits, would be an important component for realizing fully scalable, three-dimensional (3D) electro-optical integrated circuits.

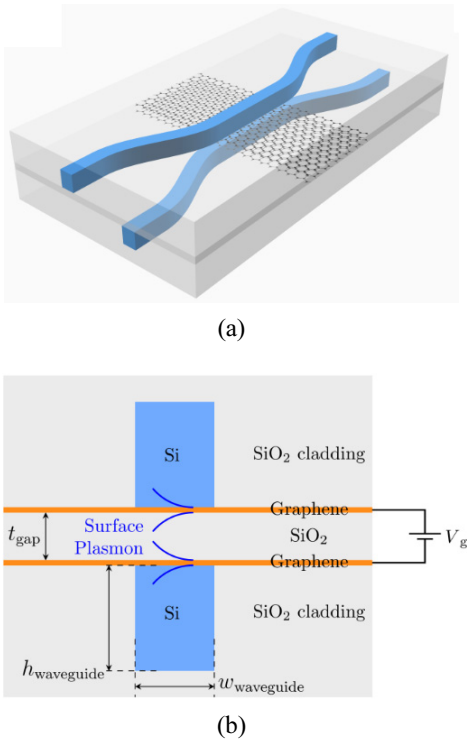

FIG. 1. (a) 3D representation of the vertically coupled directional coupler based on graphene assisted FTIR, (b) Cross-sectional view of the device in the coupling region.

II. STRUCTURE OF A VERTICAL DIRECTIONAL COUPLER BASED ON THE GA-FTIR CONFIGURATION

Figure 1(a) and 1(b) respectively present the schematic diagram of the proposed device and the 2D cross-sectional view in the coupling region. The device is comprised of two curved, vertically coupled Si waveguides (represented in blue) and two graphene layers (black) in the coupling region, separated by a thin SiO_2 layer (grey), which serves as both the FTIR potential barrier and the electrical insulator to modulate the chemical potential of the graphene layers. The device is clad entirely in SiO_2. Switching is realized by applying an electrical gate voltage between the two graphene layers.

The fundamental operation of the device is similar to that of a traditional directional coupler. Due to coupling between the two waveguides, supermodes with different effective indices exist in the coupled region. Because of the difference in effective indices, supermodes can interfere with each other as they propagate. When only one even and one odd supermode are allowed in the coupling region, constructive interference at one waveguide accompanies destructive interference at the other waveguide simultaneously. By controlling the phase difference between the even and odd supermodes, one can potentially control the amount of power coupled to the output of each waveguide.

III. SIMULATION RESULTS AND DISCUSSION

In our device, the thickness of the SiO_2 layer is fixed at t_{gap} = 10 nm. Graphene's permittivity was calculated using the Kubo formulation [15], with graphene thickness of 1 nm, Fermi velocity $V_F = 10^6$ ms^{-1}, and electron mobility $\mu = 2$ m^{2}V^{-1}s^{-1}.

To investigate the behavior of the device, we first set the width and height of the waveguides to $w_{waveguide}$ = 300 nm and $h_{waveguide}$ = 500 nm respectively. These dimensions are chosen to ensure that the guided wave is a single mode of predominantly TM polarization in the bending region.

Figure 2 shows the calculated dispersion relation of the supermodes of a 500-nm-thick coupled slab waveguide, for two different graphene chemical potentials of 0.84 eV (dashed line) and 0.90 eV (solid line). This 1D calculation is only for explaining the operating principle of the proposed device; 2D waveguide analysis was performed for the device design, as presented below. In the dispersion plot, frequency and wave number are normalized by the ENZ frequency of graphene at the chemical potential E_F = 0.90 eV. The black dash-dot line (horizontal) represents the ENZ frequency of graphene at E_F = 0.84 eV, which is the operating frequency of the device. While the dispersion curves of the even supermodes for different graphene chemical potentials (blue and red) show different behaviors, the dispersion curves of the odd supermodes (green) overlap

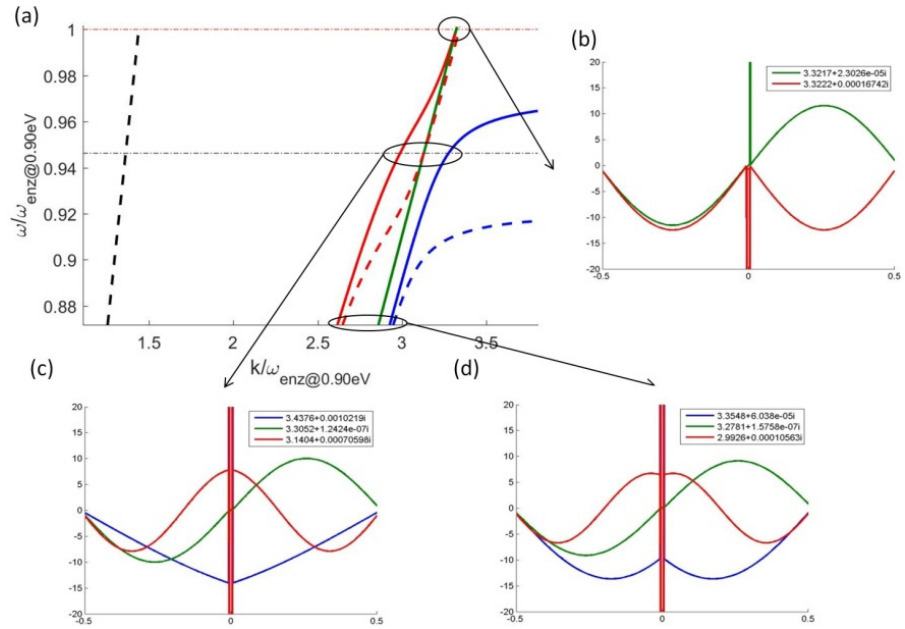

FIG. 2. (a) Dispersion relations of the coupled waveguide, for a 500-nm-thick input slab waveguide, with first-order (even symmetry), second-order (odd symmetry), and third-order (even symmetry) supermodes represented by blue, green, and red curves respectively. Frequency and wave number are normalized by the ENZ frequency of graphene at E_F = 0.90 eV. Dashed lines and solid lines correspond to graphene chemical potentials of 0.84 and 0.90 eV respectively. The black dashed line corresponds to the light line of SiO_2. (b), (c) and (d) are the cross-sectional field profiles of the waveguide for a graphene chemical potential E_F = 0.9 eV, at (b) the ENZ point of graphene at E_F = 0.90 eV, (c) ENZ point of graphene at E_F = 0.84 eV (the optimal-coupling point), and (d) far from both ENZ points. Note that the dispersion curves of the odd supermode for different graphene chemical potentials overlap each other exactly.

each other exactly. This is because the odd supermode has very low field intensity in the low-index region (SiO_2), and thus is almost unaffected by the change of coupling strength between waveguides due to changing chemical potential of graphene.

Let us consider the dispersion curves for E_F = 0.90 eV (blue, green, and red solid lines). At the ENZ frequency for E_F = 0.90 eV (red dash-dot horizontal line), the dispersion curves of the third-order (even; red) and second-order (odd; green) supermodes coincide at the same wave number, implying that those supermodes have the same effective index. This is because there is almost no coupling between waveguides at the ENZ frequency [11]. The first-order (even) supermode, associated with the ENZ mode [16] has an extremely large effective index, owing to strong field confinement in the graphene layers, such that it almost does not interfere with the other two modes. The field profiles of the second- and third-order supermodes are shown in Fig. 2(b). It can be seen that simultaneous excitation of those two supermodes from one waveguide will cancel each other completely in the waveguide, so that no optical energy is transferred between the waveguides. At the operating frequency (corresponding to the ENZ frequency for E_F = 0.84 eV; black dash-dot horizontal line), however, the first-order supermode has a finite effective index, and all three supermodes have different effective indices. The corresponding field profiles of the three supermodes are shown in Fig. 2c. At this frequency, the incident wave from one of the waveguides excites mainly the first- and second-order supermodes, while the third-order supermode's excitation is very small, because its profile has a nodal point in the waveguide region. As such, optical energy is transferred between waveguides as a result of the interference between the first- and second-order supermodes.

If similarly we consider the dispersion curves for E_F = 0.84 eV, at the operating frequency (its own ENZ frequency) the second and third supermodes coincide, and the first supermode shows an extreme large effective index. No energy transfer between waveguides occurs. Therefore, at the operating frequency the effective-index difference between two interfering supermodes can be varied from (almost) zero to a finite value, by changing the graphene chemical potential from 0.84 to 0.90 eV. Since the optimal beating length of a directional coupler is inversely proportional to the effective-index difference between even and odd supermodes, for a fixed length of coupling region, the optical output power ratio can be varied by changing the graphene chemical potential, which is easily achieved by applying a gate voltage between the graphene layers in the proposed device.

For a ridge input waveguide (as described in Fig. 1a) with $w_{waveguide}$ = 500 nm and $h_{waveguide}$ = 300 nm, the field profile and effective indices of the supermodes are described in Fig. 3. Note that propagation lengths of all supermodes

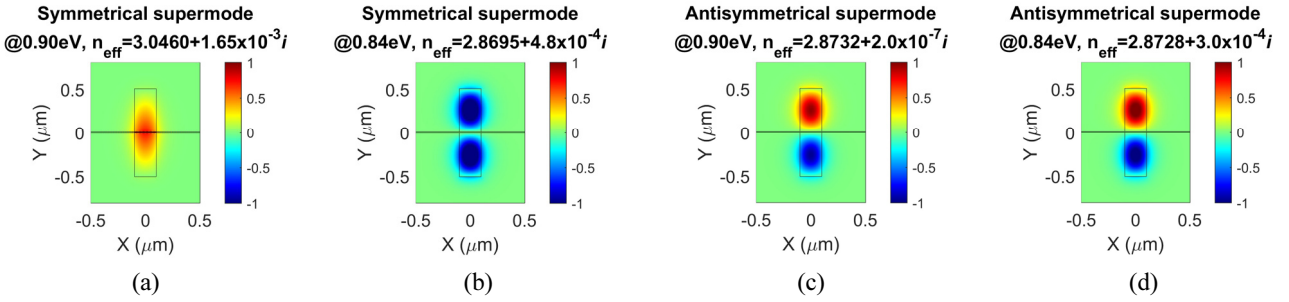

FIG. 3. FEM 2D electric-field (E_y) distribution and effective indices of different supermodes, at the operating wavelength $\lambda_0 = 1010$ nm, for a ridge input waveguide with $w_{\text{waveguide}} = 500$ nm and $h_{\text{waveguide}} = 300$ nm. (a) and (c) show the even and odd supermodes respectively, at a graphene chemical potential $E_F = 0.90$ eV. (b) and (d) show the even and odd supermodes respectively, at $E_F = 0.84$ eV, where graphene act as an ENZ material at the operating wavelength.

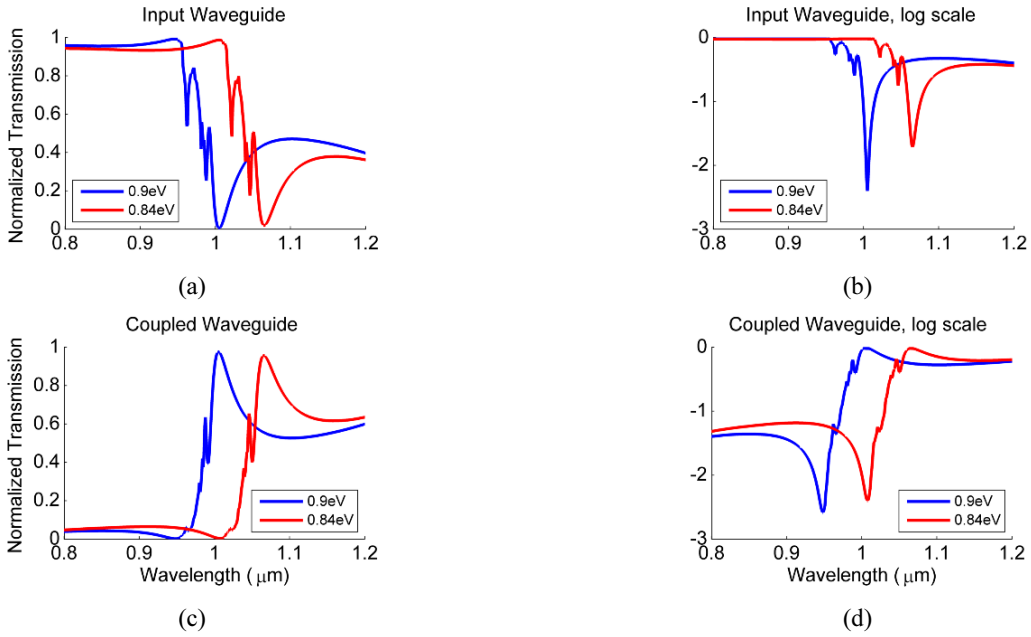

FIG. 4. FDTD calculation of the device's transmission at different graphene chemical potentials. (a) and (b) show the normalized transmission of the input waveguide, and (c) and (d) that of the coupled waveguide. (a) and (c) are plotted in linear scale, while (b) and (d) are in log scale, for visualization.

at all chemical potentials are several orders of magnitude longer than the wavelength, ensuring nearly lossless operation of the device. The optimal beating length of the two supermodes is given by $L_c = \lambda_0/(2(n_e-n_o))$ [10], where λ_0 is the operating wavelength, and n_e and n_o are the indices of the even and odd supermodes respectively. For $n_e = 3.0460$, $n_o = 2.8732$, and $\lambda_0 = 1010$ nm, the optimal beating length $L_c = 2922.5$ nm. However, due to the bending effect, the coupling length of the device cannot be exactly defined, and is numerically optimized using the FDTD method.

Figure 4 shows the device's transmission spectra for both the input channel (top channel, Fig. 4a) and the coupled channel (bottom channel, Fig. 4c), at $E_F = 0.90$ (blue curves) and 0.84 eV (red curves). Due to the very low minimum transmission at the "off" position, for clarity log-scale plots of the same spectra are also presented (Figs. 4b and 4d). Switching behavior can be observed at $\lambda_0 = 1010$ nm. Fluctuations in the spectra are due to interference among the three supermodes; however, one of the even supermodes disappears at the ENZ points, enabling proper operation of the device as designed.

Figure 5 plot the field intensity of the device at the operating wavelength $\lambda_0 = 1010$ nm, at different graphene chemical potentials $E_F = 0.90$ and 0.84 eV. At $E_F = 0.84$ eV nearly no light is transmitted to the coupled waveguide, whereas at 0.90 eV nearly all of the light is transmitted. We also observe that the straight coupling part of the device is actually shorter than the calculated beating length, due to some coupling within the bent part of the waveguides. In no-coupling (blocked) mode, the insertion loss of the input waveguide at $\lambda_0 = 1010$ nm and $E_F = 0.84$ eV is 0.06 dB, and the blocking modulation depth (the ratio of trans-

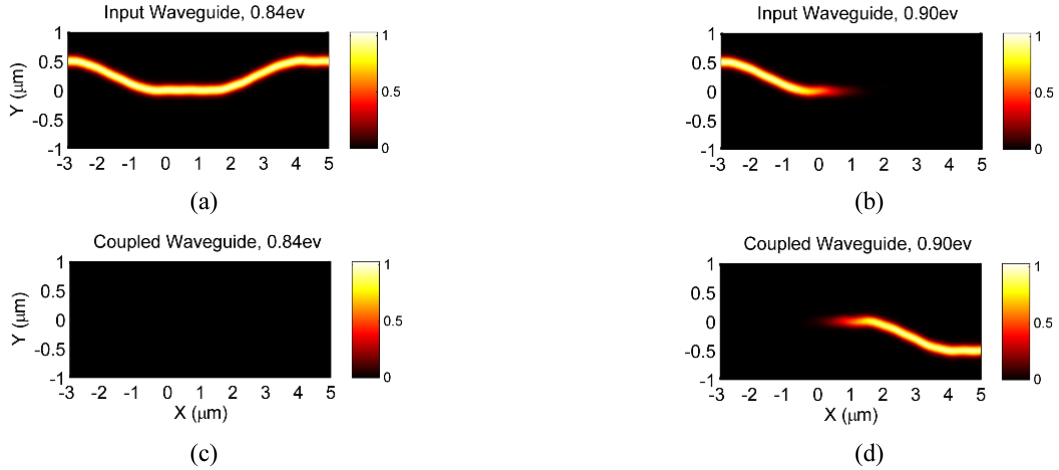

FIG. 5. FDTD calculation of the field intensity inside the device at different graphene chemical potentials E_F = 0.90 and 0.84 eV. (a) and (b) depict the field intensity of the input waveguide, and (c) and (d) that of the coupled waveguide. The operating wavelength is λ_0 = 1010 nm.

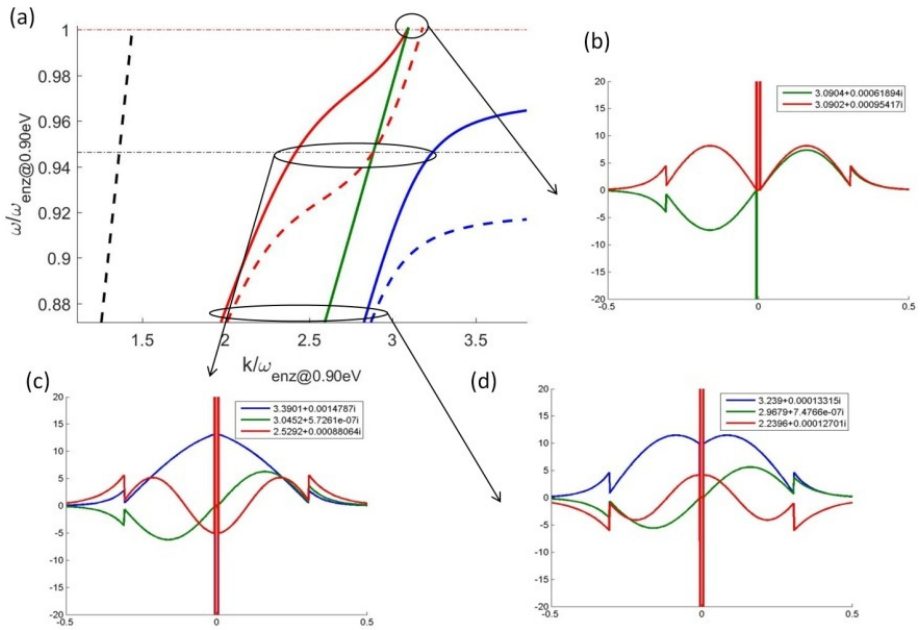

FIG. 6. (a) Dispersion relations of the coupled waveguide, for a 300-nm-thick input slab waveguide. Dashed lines and solid lines correspond to graphene chemical potentials of 0.84 and 0.90 eV respectively. (b), (c), and (d) show the cross-sectional field profile of the waveguide for a graphene chemical potential of 0.9 eV. All legends are the same as in Fig. 2.

mitted power to unwanted coupled power) is 24.0 dB. In coupled mode, the power loss when transmitted to the coupled waveguide at λ_0 = 1010 nm and E_F = 0.90 eV is 0.11 dB, and the coupled modulation depth (the ratio of coupled power to unwanted input-waveguide residual power) is 24.0 dB. Note that in both coupled and blocked modes, losses are very low, while modulation depth remains very high. Also note that it is possible to operate the device at a different wavelength (within a limited band) simply by changing the chemical potential of graphene, albeit at a cost to operating performance.

It is also possible to shorten the operating length of the device by reducing the dimensions of the input waveguide, at the cost of some reduction of the extinction ratio. To illustrate this point, a similar calculation was done on another device with waveguide dimensions $w_{\text{waveguide}}$ = 300 nm and $h_{\text{waveguide}}$ = 100 nm. Figure 6 plots the 1D dispersion relation of the supermodes of a 300-nm-thick coupled slab waveguide, for different graphene chemical potentials of 0.84 and 0.90 eV. As expected, the spread in dispersion of the supermodes grows when the input waveguide is smaller, due to better confinement and stronger interaction

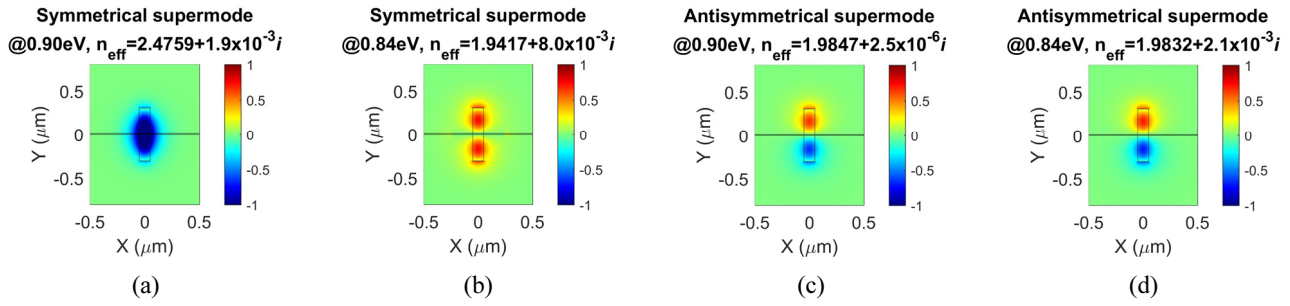

FIG. 7. FEM 2D electric field (E_y) distributions and effective indices of different supermodes, at the operating wavelength λ_0 = 1010 nm, for a ridge input waveguide with $w_{waveguide}$ = 300 nm and $h_{waveguide}$ = 100 nm. All legends are the same as in Fig. 3.

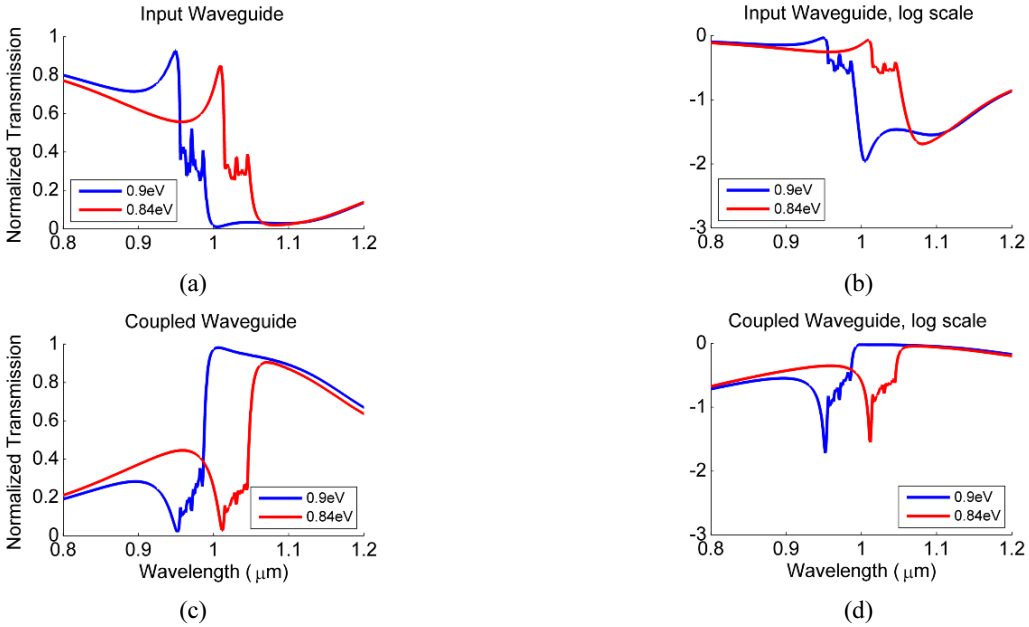

FIG. 8. FDTD calculation of the transmission at different graphene chemical potentials, for a device with $w_{waveguide}$ = 300 nm and $h_{waveguide}$ = 100 nm. Figure legends are the same as in Fig. 4.

with graphene. Otherwise, the behavior of the device is largely the same: weak interaction far from the ENZ points, an optimal coupling point where the shift of the dispersion curve is largest, and nearly zero difference at the ENZ point.

Figure 7 plots the field distribution of the smaller waveguide using the finite element method (FEM). Notice that the index difference between the supermodes at the ENZ point (E_F = 0.84 eV) is quite large, because the modes inside the more compact waveguide are not purely TM polarized, but a combination of TE and TM, *i.e.* hybrid modes. TE polarized waves are not affected by the scheme and thus provide some residual coupling between the two waveguides, reducing the overall performance of the device.

Applying the same formula [10] for n_e = 2.4759, n_o = 1.9847, and λ_0 = 1010 nm, the optimal beating length is L_c = 1028.1 nm. Note that careful optimization is required, because shortening the device would involve a sharper bending angle, which would introduce additional bending losses. Figure 8 plots the transmission spectra of the device at E_F = 0.84 and 0.90 eV. As we can see, the performance of the 300 nm by 100 nm device is somewhat worse than that of the 500 nm by 300 nm device, mainly due to the reduced optical-isolation capability of the ENZ effect, which is the result of the aforementioned residual coupling effect. On the other hand, the efficiency of power transfer to the coupled waveguide is not so affected.

Figure 9 plots the field intensity of the device at the operating wavelength λ_0 = 1010 nm, for different graphene chemical potentials E_F = 0.84 and 0.90 eV. Note that the straight coupling part of the directional coupler is all but gone, due to the highly compact nature of the device. In no-coupling (blocked) mode, the insertion loss of the input waveguide at λ_0 = 1010 nm and E_F = 0.84 eV is 0.7 dB, and the blocking modulation depth is 15.5 dB. In coupled mode, the power loss when transmitted to the coupled waveguide at λ_0 = 1010 nm and E_F = 0.90 eV is 0.08 dB, and the coupled modulation depth is 19.6 dB.

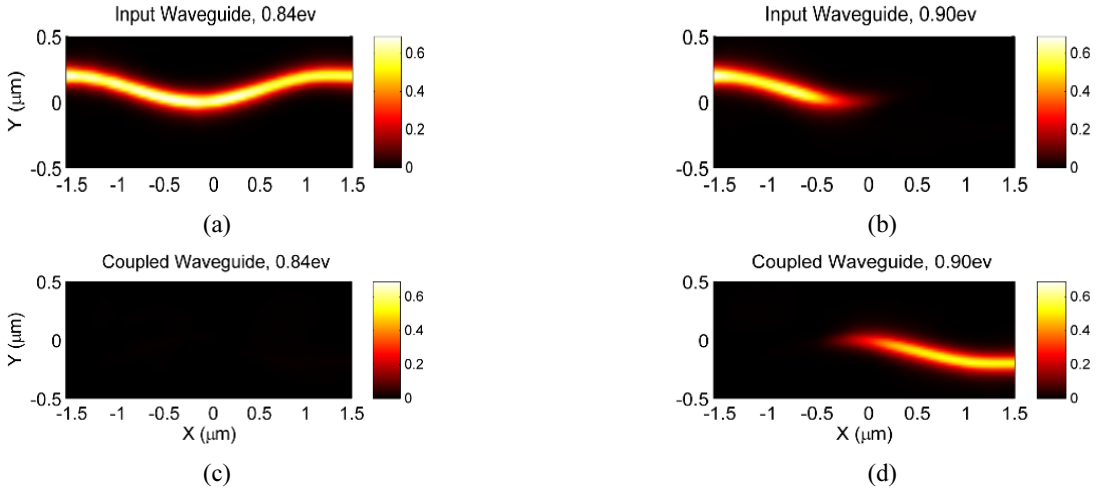

FIG. 9. FDTD calculation of the field intensity inside the device at different graphene chemical potentials E_F = 0.84 and 0.90 eV, for a device with $w_{waveguide}$ = 300 nm and $h_{waveguide}$ = 100 nm. The operating wavelength is λ_0 = 1010 nm.

IV. CONCLUSION

We propose a nearly lossless, electrically tunable vertically coupled directional coupler, based on the graphene-assisted FTIR effect. The relatively compact device (L_c≈3 μm by 1 μm) can operate with very low losses (≈0.11 dB) for both blocking and coupling states, while having a strong 24-dB extinction ratio. An even more compact device is also possible, as demonstrated, at a cost of some performance.

One of most important performance metrics for an optical modulator is modulation speed. In our devices, the modulation speed is mainly determined by the capacitance arising from the two graphene layers. To estimate the modulation speed of our device, we refer to the optical modulator demonstrated by Phare *et al.* [17], which was also based on electrical gating of graphene. In their device the total gated graphene area was approximately 1.5 μm by 30 μm, the gap distance between two graphene layers was 65 nm, and the resulting modulation speed was 30 GHz. In our devices, based on the similar electrical gating structure, the required graphene areas are 0.3 μm by 3 μm for the first device and 0.1 μm by 1 μm for the second device, while the gap distance is 10 nm, so the capacitance should decrease by factors of 7.7 and 69 for the first and second devices respectively. Their maximum modulation speeds should be correspondingly increased by the same factors.

Our previous work [11] showed that the operation of the GA-FTIR scheme at the telecommunication wavelength of 1.55 μm is possible by changing the chemical potential of graphene correspondingly. The performance of the GA-FTIR degrades slightly, since the optical-isolation effect of ENZ graphene is somewhat lowered at a chemical potential of 0.54 eV (corresponding to the ENZ of graphene at 1.55 μm). However, this effect can be compensated by increasing the number of graphene layers, as previously discussed [11], so our proposed devices can also operate at the optical communication wavelength, without considerable performance degradation.

Electrically modulated, lossless waveguide-based directional couplers could allow deep modulation of strong optical signals without any thermal build up due to optical losses, while remaining compatible with industry-standard silicon-on-insulator processes. Such devices could be an important building block for large-scale integrated 3D optical circuitry in the future.

ACKNOWLEDGMENT

This work was supported by the research fund of Signal Intelligence Research Center, supervised by Defense Acquisition Program Administration and Agency for Defense Development of Korea.

REFERENCES

1. G. T. Reed, G. Mashanovich, F. Y. Gardes, and D. J. Thomson, "Silicon optical modulators," Nat. Phot. **4**, 518-526 (2010).
2. F. Bonaccorso, Z. Sun, T. Hasan, and A. C. Ferrari, "Graphene photonics and optoelectronics," Nat. Phot. 4, 611-622 (2010).
3. J. Gosciniak and D. T. H. Tan, "Theoretical investigation of graphene-based photonic modulators," Sci. Rep. **3**, 1897 (2013).
4. X. He, "Tunable terahertz graphene metamaterials," Carbon **82**, 229-237 (2015).
5. S. H. Lee, M. Choi, T.-T. Kim, S. Lee, M. Liu, X. Yin, H. K. Choi, S. S. Lee, C.-G. Choi, S.-Y. Choi, X. Zhang, and B. Min, "Switching terahertz waves with gate-controlled active graphene metamaterials," Nat. Mater. **11**, 936-941 (2012).
6. M. Liu, X. Yin, and X. Zhang, "Double-Layer Graphene

Optical Modulator," Nano Lett. **12**, 1482-1485 (2012).
7. M. Liu, X. Yin, E. Ulin-Avila, B. Geng, T. Zentgraf, L. Ju, F. Wang, and X. Zhang, "A graphene-based broadband optical modulator," Nature **474**, 64-67 (2011).
8. R. P. Webb, R. J. Manning, G. D. Maxwell, and A. J. Poustie, "40 Gbit/s all-optical XOR gate based on hybrid-integrated Mach-Zehnder interferometer," Electron. Lett. **39**, 79-81 (2003).
9. T. Baba, S. Akiyama, M. Imai, N. Hirayama, H. Takahashi, Y. Noguchi, T. Horikawa, and T. Usuki, "50-Gb/s ring-resonator-based silicon modulator," Opt. Express **21**, 11869-11876 (2013).
10. W. Xu, Z. H. Zhu, K. Liu, J. F. Zhang, X. D. Yuan, Q. S. Lu, and S. Q. Qin, "Toward integrated electrically controllable directional coupling based on dielectric loaded graphene plasmonic waveguide," Opt. Lett. **40**, 1603-1606 (2015).
11. T. Q. Tran, S. Lee, H. Heo, and S. Kim, "Tunable Wide-Angle Tunneling in Graphene-Assisted Frustrated Total Internal Reflection," Sci. Rep. **6**, 19975 (2016).
12. J. U. Knickerbocker, P. S. Andry, B. Dang, R. R. Horton, C. S. Patel, R. J. Polastre, K. Sakuma, E. S. Sprogis, C. K. Tsang, B. C. Webb, and S. L. Wright, "3D silicon integration," Electron. Components Technol. Conf. 2008. ECTC 2008. **58th** 538-543 (2008).
13. A. W. Topol, D. C. L. Tulipe, L. Shi, D. J. Frank, K. Bernstein, S. E. Steen, A. Kumar, G. U. Singco, A. M. Young, K. W. Guarini, and M. Ieong, "Three-dimensional integrated circuits," IBM J. Res. Dev. **50**, 491-506 (2006).
14. D. H. Kim, K. Athikulwongse, M. B. Healy, M. M. Hossain, M. Jung, I. Khorosh, G. Kumar, Y.-J. Lee, D. L. Lewis, T.-W. Lin, C. Liu, S. Panth, M. Pathak, M. Ren, G. Shen, T. Song, D. H. Woo, X. Zhao, J. Kim, H. Choi, G. H. Loh, H.-H. S. Lee, and S. K. Lim, "Design and Analysis of 3D-MAPS (3D Massively Parallel Processor with Stacked Memory)," Comput. IEEE Trans. **64**, 112-125 (2015).
15. F. H. L. Koppens, D. E. Chang, and F. J. García de Abajo, "Graphene Plasmonics: A Platform for Strong Light-Matter Interactions," Nano Lett. **11**, 3370-3377 (2011).
16. S. Campione, I. Brener, and F. Marquire, "Theory of epsilon-near-zero modes in ultrathin films," Phys. Rev. B **91**, 121408 (2015).
17. C. T. Phare, Y.-H. Daniel Lee, J. Cardenas, and M. Lipson, "Graphene electro-optic modulator with 30 GHz bandwidth," Nat. Phot. **9**, 511-514 (2015).